LHCb-note 2006-058

6 November 2006

Selection of $\mathrm{B}^+ \to \overline{\mathrm{D}}^0\pi^+$ and $\mathrm{B}^+ \to \overline{\mathrm{D}}^0\mu^+\nu_\mu$ to control flavour tagging in LHCb

E. Aslanides, J. Babel, J. Cogan, R. Le Gac, O. Leroy , S. Poss and A. Tsaregorodtsev

CPPM, IN2P3-CNRS et Université d'Aix-Marseille II

Abstract

The channels $\mathrm{B}^+ \to \overline{\mathrm{D}}^0\pi^+$ and $\mathrm{B}^+ \to \overline{\mathrm{D}}^0\mu^+\nu_\mu$ are studied in both signal and generic $\mathrm{b\overline{b}}$ Monte Carlo. With an integrated luminosity of $2\,\mathrm{fb}^{-1}$, we expect 1 million $\mathrm{B}^+ \to \overline{\mathrm{D}}^0\pi^+$ events triggered and selected with B/S=0.1 and 2.4 M $\mathrm{B}^+ \to \overline{\mathrm{D}}^0\mu^+\nu_\mu$ events with B/S =0.7. These channels are useful to calibrate the opposite side mistag fraction. With only $0.1\,\mathrm{fb}^{-1}$ we expect a relative uncertainty on the opposite side mistag of 0.6%.

Contents

1 Introduction

LHCb will measure B-meson CP asymmetries in order to extract fundamental parameters of the Standard Model, like the CKM phases α, β, γ and ϕ_s. One mandatory step is to determine the flavour of the B-meson at the time of its production. This "flavour tagging" is performed with an algorithm [1] exploiting information from the "same side" and the "opposite side" with respect to the B-meson entering in the CP asymmetry. The mistag rate has to be extracted from "control channels" with flavour-specific final state. Many channels have already been studied in LHCb like $B_s^0 \to D_s^- \pi^+$ [2], $B^+ \to J/\psi K^+$ [3] and $B^0 \to D^{*-} \mu^+ \nu_\mu$. In this note, we propose two new B^+ modes useful to measure the opposite side mistag rate: $B^+ \to \overline{D}^0 \mu^+ \nu_\mu$ and $B^+ \to \overline{D}^0 \pi^+$ [4]. They are interesting because of their large visible branching ratio and because the charge of the final state should allow an easy measurement of the mistag rate, provided the background is under control. At the end, the best precision on the mistag rate will come from a combination of several channels.

In Section 2, we present the simulation used to produce signal and background events. In Section 3, we describe the selection of the events including the proper time measurement. Section 4 is devoted to the event yield for one year of data taking as well as the estimation of the background over signal ratio. Eventually, in Section 5, we explain how useful these channels are to measure the opposite side mistag.

2 Monte Carlo event samples

The topologies of $B^+ \to \overline{D}^0 \pi^+$ and $B^+ \to \overline{D}^0 \mu^+ \nu_\mu$ are indicated on Figs. 1 and 2. For sake of simplicity, we only reconstruct the $\overline{D}^0$ into $K^+\pi^-$, which represents 3.8% of the $\overline{D}^0$ decays.

The events are simulated using PYTHIA 6.226 [6]. The decay of particles is performed with the EvtGen program [7]. The particles are tracked through the detector material using the GEANT4 package [8], and the Gauss program [9]. The digitization is done with Boole [10] and the reconstruction with Brunel [11]. The events are analysed with DaVinci v12r18 [12] and Bender v4r8p5 [13].

We use two signal and one background samples[1]:

- 242,000 $B^+ \to \overline{D}^0 \pi^+$ events;
- 199,500 $B^+ \to \overline{D}^0 \mu^+ \nu_\mu$ events;
- 33.9 M inclusive $b\overline{b}$ events;

The particle of interest (i.e. the signal-b hadron or one of the b-hadrons in the inclusive $b\overline{b}$ events) is required to have a true polar angle smaller than 400 mrad. The sample sizes mentioned above are given after this requirement. The efficiency of this angular cut is ε_θ^s=34.7% for signal B events and ε_θ^b=43.4% for inclusive $b\overline{b}$ events.

[1] In the Bookkeeping database, the signal corresponds to the configuration "DC04-v2r3" while the background configuration name is "Stripping-v2."

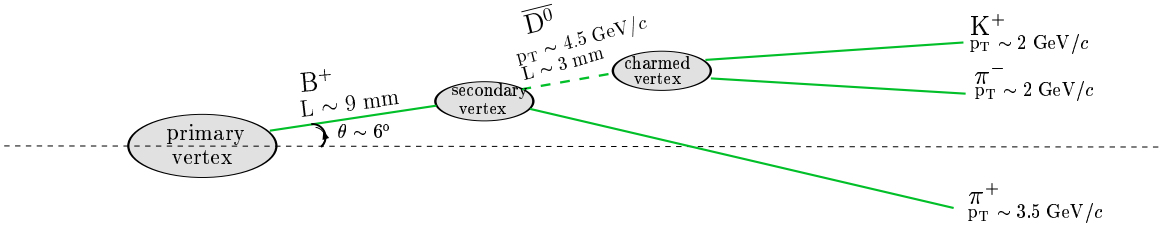

Figure 1: Topology of the $B^+ \to \overline{D}^0 \pi^+$ decay.

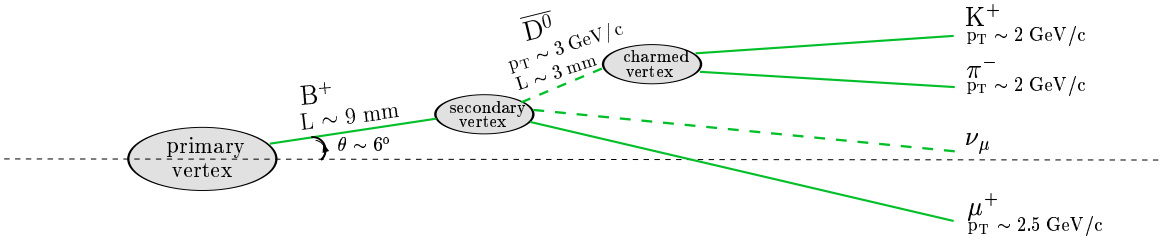

Figure 2: Topology of a $B^+ \to \overline{D}^0 \mu^+ \nu_\mu$ decay.

The exclusive visible branching ratio of the channels of interest are [5]:

$$\begin{aligned} \mathrm{BR}^{\mathrm{vis}}(B^+ \to \overline{D}^0 \pi^+) &= \mathrm{BR}(\overline{D}^0 \to K^+ \pi^-) \times \mathrm{BR}(B^+ \to \overline{D}^0 \pi^+) \\ &= 3.8\% \times 0.498\% \\ &= 1.89 \times 10^{-4}, \end{aligned} \tag{1}$$

$$\begin{aligned} \mathrm{BR}^{\mathrm{vis}}(B^+ \to \overline{D}^0 \mu^+ \nu_\mu) &= \mathrm{BR}(\overline{D}^0 \to K^+ \pi^-) \times \mathrm{BR}(B^+ \to \overline{D}^0 \mu^+ \nu_\mu) \\ &= 3.8\% \times 2.15\% \\ &= 8.17 \times 10^{-4}. \end{aligned} \tag{2}$$

In comparison, the highest visible branching ratio of the B^+ modes studied so far in LHCb is: $\mathrm{BR}^{\mathrm{vis}}(B^+ \to J/\psi K^+) = 0.68 \times 10^{-4}$.

3 Events Selection

The selection algorithms are designed to select the largest number of signal events, while keeping the background level under control. The reconstruction of the primary vertex candidates is described in [14] (page 88).

3.1 Selection of $B^+ \to \overline{D}^0\pi^+$ events

Figures 3 to 10 show the distribution of kinematic variables of interest to discriminate signal from $b\overline{b}$ background events, with some very loose preselection cuts[2]. In all the plots, the distribution of signal and background is normalized to unity, for comparison. We select two opposite charge tracks identified as pion and kaon ($\Delta \ln \mathcal{L}_{K\pi} > -5.0$) and fulfilling the cuts indicated in Table 1. These tracks must form a vertex with a $\chi^2 < 25$. The invariant mass of the $K^+\pi^-$ pairs is shown on Fig. 11 . It is required to be within $50\,\mathrm{MeV}/c^2$ of the nominal $\overline{D}^0$ mass. The resolution is $6.8\,\mathrm{MeV}/c^2$. The reconstructed $\overline{D}^0$ should have transverse momentum $p_T(\overline{D}^0) > 1\,\mathrm{GeV}/c$. It is associated with a charged pion to form a B^+ candidate. We call this pion π_1 to distinguish it from the pion coming from the $\overline{D}^0$.

variable	cut
$p_T(K^+,\,\pi^-)$	$> 0.3\,\mathrm{GeV}/c$
$p(K^+,\pi^-)$	$> 2\,\mathrm{GeV}/c$
$\mathrm{ip_{PV}}/\sigma(\mathrm{ip_{PV}})(K^+,\pi^-)$	> 2
$\chi^2(K^+\pi^-)$	< 25
$m(K^+\pi^-) = m(\overline{D}^0)$	$\pm\, 50\,\mathrm{MeV}/c^2$
$p_T(\overline{D}^0)$	$> 1\,\mathrm{GeV}/c$

Table 1: Cuts applied to reconstruct $\overline{D}^0 \to K^+\pi^-$.

The final selection cuts are indicated in Table 2. The pion π_1 must have momentum greater then $10\,\mathrm{GeV}/c$ and a transverse momentum greater than $2\,\mathrm{GeV}/c$. The reconstructed $\overline{D}^0$ should have momentum, $p(\overline{D}^0) > 20\,\mathrm{GeV}/c$ and a transverse momentum, $p_T(\overline{D}^0) > 2.5\,\mathrm{GeV}/c$. The obtained $\overline{D}^0\pi$ vertex should have a $\chi^2 < 6$ and being at least 1 mm downstream of the primary vertex along the z direction. We also require that the reconstructed $\overline{D}^0$ vertex is downstream of the reconstructed $\overline{D}^0\pi$ vertex: $z(\overline{D}^0) > z(\overline{D}^0\pi)$.

The B^+ candidate should have a momentum vector pointing back toward the primary vertex. A vector $\vec{r}$ is constructed from the positions of primary and $\overline{D}^0\pi^+$ vertex. This vector is expected to be collinear with the momentum vector $\vec{p}(\overline{D}^0\pi^+)$. A cut on

$$\cos(\theta) = \frac{\vec{p}(\overline{D}^0\pi^+)\vec{r}}{|\vec{p}(\overline{D}^0\pi^+)||\vec{r}|}$$

removes a large fraction of background, while retaining most of signal events, as shown on Fig. 9. The impact parameter significance of the B^+ candidate with respect to at least

[2]Standard loose $\overline{D}^0$ selection described in this section, $\chi^2(\overline{D}^0\pi^+) < 20$ and $m(\overline{D}^0\pi^+) = m(B^+) \pm 600\,\mathrm{MeV}/c^2$.

one primary vertex must be lower than 4. Eventually, we ask the $\overline{\mathrm{D}}^0\pi^+$ invariant mass to be compatible with the B^+ mass within $\pm 50\,\mathrm{MeV}/c^2$. Figure 12 shows the distribution of this invariant mass, obtained on the $\mathrm{B}^+ \to \overline{\mathrm{D}}^0\pi^+$ sample, fitted with a Gaussian. It is centered on the nominal B^+ mass and the resolution is $16.3\,\mathrm{MeV}/c^2$. Figure 13 shows the same distribution, obtained on the $\mathrm{b\overline{b}}$ sample, where the mass cut has been relaxed to show the partially reconstructed decays, in the lower region. These decays with intermediate resonant D-meson could certainly be exploited for tagging, in a future study.

variable	cut
$p_{\mathrm{T}}(\pi_1)$	> 2 GeV/c
$p(\pi_1)$	> 10 GeV/c
$p_{\mathrm{T}}(\overline{\mathrm{D}}^0)$	> 2.5 GeV/c
$p(\overline{\mathrm{D}}^0)$	> 20 GeV/c
$\chi^2(\overline{\mathrm{D}}^0\pi^+)$	< 6
$z(\overline{\mathrm{D}}^0) - z(\mathrm{D}^0\pi)$	$> 0\,\mathrm{mm}$
$z(\mathrm{D}^0\pi) - z(\text{primary vertex})$	$> 1\,\mathrm{mm}$
$\cos\theta$	> 0.99997
$\mathrm{ip}_{\mathrm{PV}}/\sigma(\mathrm{ip}_{\mathrm{PV}})(\overline{\mathrm{D}}^0\pi^+)$	< 4
$m(\overline{\mathrm{D}}^0\pi^+) = m(\mathrm{B}^+)$	$\pm$ 50 MeV/c^2

Table 2: Cuts applied to reconstruct $\mathrm{B}^+ \to \overline{\mathrm{D}}^0\pi_1^+$.

The final selection keeps 8957 events among 214,000[3], corresponding to an efficiency of $4.19 \pm 0.04\%$. Among those, 5101 fulfill Level-0 trigger criteria and 3951 pass Level-0 and Level-1 trigger. The trigger efficiencies are respectively $\varepsilon_{\mathrm{L0}}$=5101/8957=$56.9 \pm 0.5\%$ and $\varepsilon_{\mathrm{L0\times L1}}$=3951/8957 = $44.1 \pm 0.5\%$. The total selection efficiency after L0 and L1 is:

$$\begin{aligned} \varepsilon_{\mathrm{tot}} &= 3951/214000 \times \varepsilon_{\theta}^{\mathrm{s}} \\ &= 0.64 \pm 0.01\% \end{aligned}$$

Figure 14 gives the momentum resolution which is 0.3%. Figure 15 shows the B^+ vertex resolution along the three axis. The core of the resolution is typically 17 μm in x, y and 192 μm in z. The proper time of the B^+ candidates is computed with:

$$t = \frac{lm}{p} \tag{3}$$

where l and p are respectively the decay length and the momentum of the B^+ candidate. The proper time resolution is given in Fig. 16. It is fitted by the sum of two Gaussians. The standard deviation of 92% of the events is 41 fs, while the tails have a standard deviation 184 fs.

3.2 Selection of $\mathrm{B}^+ \to \overline{\mathrm{D}}^0\mu^+\nu_\mu$ events

The $\overline{\mathrm{D}}^0$ is reconstructed with the procedure described in the previous section. It is associated with a charged track identified as a muon ($\Delta \ln \mathcal{L}_{\pi\mu} > -15$). The B^+ can not

[3]For technical reasons of data access, we run only on the sub-sample of the 242,000 generated events.

be fully reconstructed because of the neutrino which escapes detection. Figures 17 to 19 show kinematic variables of interest to discriminate signal from $b\overline{b}$ background events.

The selection cuts are summarized in Table 3. The muon must have $p(\mu) > 10\,\mathrm{GeV}/c$, $p_{\mathrm{T}}(\mu) > 2\,\mathrm{GeV}/c$ and an impact parameter significance with respect to all primary vertices greater than 2. The $\overline{\mathrm{D}}^0$ must have $p(\overline{\mathrm{D}}^0) > 15\,\mathrm{GeV}/c$ and $p_{\mathrm{T}}(\overline{\mathrm{D}}^0) > 3\,\mathrm{GeV}/c$. The $\overline{\mathrm{D}}^0\mu^+$ vertex must have a $\chi^2 < 6$ and must be at least 1 mm away of the primary vertex in the z-direction. The impact parameter significance of the B^+ candidate with respect to the closest primary vertex must be smaller than 4. Figure 20 shows the invariant mass distribution of the $\overline{\mathrm{D}}^0\mu^+$ pair, obtained on the $\mathrm{B}^+ \to \overline{\mathrm{D}}^0\mu^+\nu_\mu$ sample. The cut on this mass, $3.5\,\mathrm{GeV}/c^2 < m(\overline{\mathrm{D}}^0\mu^+) < 6\,\mathrm{GeV}/c^2$ is very large, because of the missing neutrino. Figure 21 shows the same distribution, obtained on the $b\overline{b}$ sample, where the mass cut has been relaxed.

The final selection keeps 981 $\mathrm{B}^+ \to \overline{\mathrm{D}}^0\mu^+\nu_\mu$ events among the 199,500 generated, corresponding to an efficiency of $0.49 \pm 0.02\%$. Among those, 720 pass the Level-0 and Level-1 triggers, corresponding to an efficiency of $\varepsilon_{\mathrm{L0\times L1}} = 73.4 \pm 1.4\%$. The total selection efficiency after Level-0 and Level-1 is:

$$\begin{aligned} \varepsilon_{\mathrm{tot}} &= 720/199500 \times \varepsilon^{\mathrm{s}}_{\theta} \\ &= 0.125 \pm 0.005\% \end{aligned}$$

variable	cuts
$p_{\mathrm{T}}(\mu)$	> 2 GeV/c
$p(\mu)$	> 10 GeV/c
$\mathrm{ip_{PV}}/\sigma(\mathrm{ip_{PV}})(\mu)$	> 2
$p_{\mathrm{T}}(\overline{\mathrm{D}}^0)$	> 3 GeV/c
$p(\overline{\mathrm{D}}^0)$	> 15 GeV/c
$\chi^2(\overline{\mathrm{D}}^0\mu^+)$	< 6
$z(\overline{\mathrm{D}}^0\mu^+) - z(\text{primary vertex})$	> 1 mm
$\mathrm{ip_{PV}}/\sigma(\mathrm{ip_{PV}})(\overline{\mathrm{D}}^0\mu^+)$	< 4
$\cos\theta$	> 0.99995
$m(\overline{\mathrm{D}}^0\mu^+) \in$	[3.5 , 6] GeV/c^2

Table 3: Cut applied to reconstruct $\mathrm{B}^+ \to \overline{\mathrm{D}}^0\mu^+\nu_\mu$.

To account from the missing neutrino, we correct the reconstructed momentum of the $\overline{\mathrm{D}}^0\mu^+$ object. The correction term is a function of the $\overline{\mathrm{D}}^0\mu^+$ invariant mass: a high $\overline{\mathrm{D}}^0\mu^+$ mass means a low momentum neutrino. Figure 22 shows the correlation between $p(\overline{\mathrm{D}}^0\mu^+)/p_{\mathrm{true}}(\mathrm{B}^+)$ and the $m(\overline{\mathrm{D}}^0\mu^+)$ invariant mass. It is adjusted by a first-order polynomial function $f(m_{\overline{\mathrm{D}}^0\mu^+})$. The B^+ momentum is corrected as follows:

$$p_{\mathrm{cor}}(\overline{\mathrm{D}}^0\mu^+) = \frac{p_{\text{not cor}}(\overline{\mathrm{D}}^0\mu^+)}{f(m_{\overline{\mathrm{D}}^0\mu^+})}$$

The momentum resolution after this correction is 17%, as shown on Fig. 23. The proper time is then computed using Eq. (3). The proper time resolution is shown on Fig. 24,

fitted with the sum of two Gaussians. The standard deviation of 61% of the events is 149 fs, while the tails have a standard deviation of 613 fs.

4 Event yield calculation and background estimate

The annual event yield is given by:

$$S = \mathcal{L}_{\rm int} \times \sigma_{\rm b\overline{b}} \times {\rm BR}({\rm b} \to {\rm B}^+) \times 2 \times {\rm BR}^{\rm vis} \times \varepsilon_{\rm tot}. \quad (4)$$

The nominal annual integrated luminosity is $\mathcal{L}_{\rm int}$ =2 fb^{-1} (10^7 s at 2×10^{32} cm^{-2}s^{-1}). The b$\overline{\rm b}$ production cross section is $\sigma_{\rm b\overline{b}} = 500\,\mu$b. The probability for a $\overline{\rm b}$-quark to hadronize into a B$^+$ is BR(b$\to$ B$^+$)=40.5% [7]. The factor 2 takes into account the production of both b- and $\overline{\rm b}$-hadrons. BR$^{\rm vis}$ is the product of all branching ratios involved in the b-hadron decay of interest; $\varepsilon_{\rm tot}$ is the total efficiency, including acceptance, reconstruction, trigger and selection.

4.1 $\rm B^+ \to \overline{D}^0 \pi^+$

The annual yield of $\rm B^+ \to \overline{D}^0 \pi^+$ event is computed with Eq. (4) and $\varepsilon_{\rm tot}$=0.64 $\pm$ 0.01%. We expect 1 M triggered and selected events after Level-0 and Level-1.

The estimation of the level of background is based on 31.4 M b$\overline{\rm b}$ events[4], which corresponds to few minutes of data-taking in nominal conditions. To cope with this limited Monte Carlo statisitics, the background studies are performed without applying the trigger. Among the 31.4 M of b$\overline{\rm b}$ events, 188 events pass the selection, 166 of which are signal events. This corresponds to a background over signal ratio of:

$$\frac{B}{S} = \frac{22}{166} = 0.13 \pm 0.03.$$

The 188 events are classified in Table 4. The level of background in $\rm B^+ \to \overline{D}^0 \pi^+$ is very low. The main background is $\rm B^+ \to \overline{D}^0 K^+$, which branching ratio is 10 times smaller than $\rm B^+ \to \overline{D}^0 \pi^+$: BR($\rm B^+ \to \overline{D}^0 K^+$)= 4.1×10^{-4} [5].

4.2 $\rm B^+ \to \overline{D}^0 \mu^+ \nu_\mu$

In the $\rm B^+ \to \overline{D}^0 \mu^+ \nu_\mu$ selection described above, only the exclusive decay has been simulated. However, other similar B$^+$ decays lead to a final state with a $\overline{\rm D}^0$ and a μ^+. $\rm B^+ \to \overline{D}^{(*)0} \tau^+ \nu_\tau$ decays where $\tau^+ \to \mu^+ \nu_\mu \overline{\nu_\tau}$ and $\overline{\rm D}^{(*)0} \to \overline{\rm D}^0$X can be selected in the same way, leading to an increased statistical power. We call these modes "inclusive decays" and note them $\rm B^+ \Rightarrow \overline{D}^0 \mu^+ \nu_\mu$. To compute $\rm BR^{vis}_{incl}(B^+ \Rightarrow \overline{D}^0 \mu^+ \nu_\mu)$, we take into account $\overline{\rm D}^*(2007)^0$, $\overline{\rm D}_1(2420)^0$, $\overline{\rm D}_2^*(2460)^0$, $\overline{\rm D}_0^*(2400)^0$. With the values given in Table 5,

[4]For technical reasons of data access, we run only on 92.6% of the full b$\overline{\rm b}$ statistics.

Monte Carlo truth	Number of selected events
$B^+ \to \overline{D}^0 \pi^+$	166
$B^+ \to \overline{D}^0 K^+$	8
$B^+ \to \overline{D}^0 \pi^+$(wrong charge)	2
$B^0 \to D^{*-} e^+ \nu_e$	2
$B^0 \to D^{*-} \pi^- \mu^+ \nu_\mu$	1
$B^+ \to J/\psi(\mu\mu) K^+$	1
$\Lambda_b \to \Lambda_c^- \pi^+$	1
$B^0 \to D^{*-} D_s^{*+}$	1
$B^0 \to D^{*-} \tau^+ \nu_\tau$	1
$B^+ \to \rho^+ \pi^+ \pi^-$	1
$\Lambda_b \to \Lambda_c^- \tau^+ \nu_\tau$	1
$B^+ \to \overline{D}^0 \mu^+ \nu_\mu$	1
$B^+ \to \bar{\rho}^0 \pi^+$	1
$B^+ \to \overline{D}^{(*)0} \pi^0 \bar{\rho}^0 \pi^+$	1

Table 4: Detail of the 188 $B^+ \to \overline{D}^0 \pi^+$ candidates selected among the 33.9 M $b\overline{b}$ events.

the inclusive branching ratio of $B^+ \Rightarrow \overline{D}^0 \mu^+ \nu_\mu$ is:

$$\begin{aligned} BR^{vis}_{incl}(B^+ \Rightarrow \overline{D}^0 \mu^+ \nu_\mu) &= BR(B^+ \to \overline{D}^{(*)0}_{1,2} \mu^+ \nu_\mu) \times BR(\overline{D}^{(*)0}_{1,2} \Rightarrow \overline{D}^0 X) \times BR(\overline{D}^0 \to K^+ \pi^-) \\ &+ BR(B^+ \to \overline{D}^{(*)0}_{1,2} \tau^+ \nu_\tau) \times BR(\tau^+ \to \mu^+ \nu_\mu \overline{\nu_\tau}) \times BR(\overline{D}^{(*)0}_{1,2} \Rightarrow \overline{D}^0 X) \\ &\times BR(\overline{D}^0 \to K^+ \pi^-) \\ &= 0.083 \times 0.038 + 0.025 \times 0.1734 \times 0.038 \\ &= 3.32 \times 10^{-3}. \end{aligned} \quad (5)$$

It is about 4 times larger than the exclusive $BR^{vis}_{excl}(B^+ \to \overline{D}^0 \mu^+ \nu_\mu)$.

Among the 33.9 M generated $b\overline{b}$ events, 446 events pass the selection cuts and are classified in Table 6. Among these, 255 correspond to $B^+ \Rightarrow \overline{D}^0 \mu^+ \nu_\mu$ decays. The background over signal ratio is:

$$\frac{B}{S} = \frac{191}{255} = 0.75 \pm 0.03.$$

Notice that 65% of the background is due to neutral $B^0 \to D^{*-} \mu^+ \nu_\mu$ decays.

To compute the annual yield of $B^+ \Rightarrow \overline{D}^0 \mu^+ \nu_\mu$ events with Eq. (4), we need the total selection efficiency of *inclusive* decays. In Sect. 3.2, we computed the selection efficiency of *exclusive* $B^+ \to \overline{D}^0 \mu^+ \nu_\mu$ decays: ε_{tot}(excl, from signal)=$0.125 \pm 0.005\%$. We check this efficiency is compatible with the one extracted from the $b\overline{b}$ sample:

$$\varepsilon_{tot}(\text{excl, from } b\overline{b}) = \frac{79 \times \varepsilon_{L0\times L1}(\text{excl}) \times \varepsilon^b_\theta}{2 \times BR(b \to B^+) \times BR^{vis}_{excl}(B^+ \to \overline{D}^0 \mu^+ \nu_\mu) \times 33.9\,M} = 0.11 \pm 0.02\%$$

The selection efficiency on *inclusive* $B^+ \Rightarrow \overline{D}^0 \mu^+ \nu_\mu$ is:

$$\varepsilon_{tot}(\text{incl, from } b\overline{b}) = \frac{255 \times \varepsilon_{L0\times L1}(\text{incl}) \times \varepsilon^b_\theta}{2 \times BR(b \to B^+) \times BR^{vis}_{incl}(B^+ \Rightarrow \overline{D}^0 \mu^+ \nu_\mu) \times 33.9\,M} = 0.09 \pm 0.01\%$$

$BR(\overline{D}^0 \to K^+\pi^-)$	3.8%
$BR(B^+ \to \overline{D}^0\mu^+\nu_\mu)$	2.1%
$BR(B^+ \to \overline{D}^{*0}\mu^+\nu_\mu)$	5.6%
$BR(B^+ \to \overline{D}_1(2420)^0\mu^+\nu_\mu)$	0.44%
$BR(B^+ \to \overline{D}_0^{*0}\mu^+\nu_\mu)$	0.066%
$BR(B^+ \to \overline{D'}_1^0\mu^+\nu_\mu)$	0.29%
$BR(B^+ \to \overline{D}_2^{*0}\mu^+\nu_\mu)$	0.176%
$BR(B^+ \to \overline{D}^0\tau^+\nu_\tau)$	1.6%
$BR(B^+ \to \overline{D}^{*0}\tau^+\nu_\tau)$	0.7%
$BR(B^+ \to \overline{D}_1(2420)^0\tau^+\nu_\tau)$	0.103%
$BR(B^+ \to \overline{D}_0^{*0}\tau^+\nu_\tau)$	0.043%
$BR(B^+ \to \overline{D'}_1^0\tau^+\nu_\tau)$	0.158%
$BR(B^+ \to \overline{D}_2^{*0}\tau^+\nu_\tau)$	0.095%
$BR(\overline{D}_1(2420)^0 \to \overline{D}^{*0}\pi^0)$	33.33%
$BR(\overline{D}_1(2420)^0 \to D^{*+}\pi^-)$	45.54%
$BR(D^{*+} \to \overline{D}^0\pi^+)$	68%
$BR(\overline{D}_0^{*0} \to \overline{D}^0\pi^0)$	33.3%
$BR(\overline{D'}_1^0 \to D^{*+}\pi^-)$	45.54%
$BR(\overline{D'}_1^0 \to \overline{D}^{*0}\pi^0)$	33.3%
$BR(\overline{D}_2^{*0} \to D^{*+}\pi^-)$	14.27%
$BR(\overline{D}_2^{*0} \to \overline{D}^{*0}\pi^0)$	10.3%
$BR(\overline{D}_2^{*0} \to \overline{D}^0\pi^0)$	22.9%
$BR(\tau^+ \to \mu^+\nu_\mu\overline{\nu}_\tau)$	17.31%

Table 5: Values used to compute inclusive branching ratio $B^+ \Rightarrow \overline{D}^0\mu^+\nu_\mu$ [5, 7].

Monte Carlo truth	Number of selected events
$B^+ \Rightarrow \overline{D}^0\mu^+\nu_\mu$ (without $B^+ \to \overline{D}^0\mu^+\nu_\mu$)	176
$B^+ \to \overline{D}^0\mu^+\nu_\mu$	79
$B^0 \Rightarrow D^{*-}\mu^+\nu_\mu$	124
$B_d^0 \to D^{*0}\pi^-\mu^+\nu_\mu$	20
$B_d^0 \to D^0\pi^-\mu^+\nu_\mu$	7
$B_d^0 \to K^{*+}J/\psi\rho^-$	3
$B_d^0 \to D^-\mu^+\nu_\mu$	1
other	36

Table 6: Detail of the 446 $B^+ \to \overline{D}^0\mu^+\nu_\mu$ candidates selected in the 33.9 M $b\overline{b}$ sample.

where we measure $\varepsilon_{\mathrm{L0\times L1}}(\mathrm{incl}) = 73 \pm 3\%$ in the $\mathrm{b\overline{b}}$ sample.

Therefore, we expect an annual yield of 2.4 M triggered and selected $\mathrm{B}^+ \Rightarrow \overline{\mathrm{D}}^0\mu^+\nu_\mu$ events per year.

5 Opposite side mistag extraction

mode	annual yield	B/S	$\varepsilon_{\mathrm{OS}}$ (%) from MC	ω_{OS}(%) from MC	$\sigma(\omega_{\mathrm{OS}})/\omega_{\mathrm{OS}}$ (%) extrapolated with $\mathcal{L}_{\mathrm{int}} = 2\,\mathrm{fb}^{-1}$
$\mathrm{B}^+ \to \mathrm{J}/\psi\mathrm{K}^+$	1.74 M	0.4	43.4 ± 0.1	36.7 ± 0.4	0.15
$\mathrm{B}^+ \Rightarrow \overline{\mathrm{D}}^0\mu^+\nu_\mu$	2.4 M	0.7	47.1 ± 1.9	36.8 ± 2.7	0.12
$\mathrm{B}^+ \to \overline{\mathrm{D}}^0\pi^+$	1 M	0.1	44.7 ± 0.5	36.4 ± 1.5	0.20

Table 7: After L0×L1 trigger and offline selection, we give the expected annual yield and B/S estimated from the inclusive $\mathrm{b\overline{b}}$ sample, for the charged modes $\mathrm{B}^+ \to \mathrm{J}/\psi\mathrm{K}^+$, $\mathrm{B}^+ \to \overline{\mathrm{D}}^0\pi^+$ and $\mathrm{B}^+ \Rightarrow \overline{\mathrm{D}}^0\mu^+\nu_\mu$. The opposite side mistag performance ($\varepsilon_{\mathrm{OS}}$, ω_{OS}) are estimated from the simulation of the exclusive decays. In the last column, the relative uncertainty on ω_{OS} is extrapolated for $\mathcal{L}_{\mathrm{int}} = 2\,\mathrm{fb}^{-1}$, ignoring background.

Table 7 summarizes the yield and B/S for the charged modes $\mathrm{B}^+ \to \mathrm{J}/\psi\mathrm{K}^+$, $\mathrm{B}^+ \to \overline{\mathrm{D}}^0\pi^+$ and $\mathrm{B}^+ \Rightarrow \overline{\mathrm{D}}^0\mu^+\nu_\mu$. The opposite side tagging efficiency, $\varepsilon_{\mathrm{OS}}$, and opposite side mistag rate, ω_{OS}, are estimated from the simulation of exclusive decays. The mistag fraction is computed comparing the result of the opposite side tagging algorithm with the flavour of the *reconstructed* final state[5].

Figure 25 shows the evolution of the relative uncertainty on the opposite side mistag rate as a function of the integrated luminosity, for the three charged modes. It is obtained with the following formula:

$$\sigma(\omega_{OS})^2 = \frac{\omega_{OS} \times (1 - \omega_{OS})}{\varepsilon_{\mathrm{OS}} \times S(\mathcal{L}_{\mathrm{int}})}$$

ignoring the background contribution. $S(\mathcal{L}_{\mathrm{int}})$ is given by Eq. (4).

An integrated luminosity of $0.1\,\mathrm{fb}^{-1}$ would allow the extraction of ω_{OS} with a relative statistical uncertainty of 0.6%, using $\mathrm{B}^+ \Rightarrow \overline{\mathrm{D}}^0\mu^+\nu_\mu$ alone. In comparison, $\mathrm{B}^+ \to \mathrm{J}/\psi\mathrm{K}^+$ would allow the extraction of ω_{OS} with a relative statistical uncertainty of 0.7%. In practice, the use of control channels will be decided on more complicated criteria than just statistical considerations. We must take into account how the channels are triggered and the phase space correlations between control and signal channels [15].

In addition, background brings other uncertainty in the mistag extraction. We will illustrate this with the $\mathrm{B}^+ \Rightarrow \overline{\mathrm{D}}^0\mu^+\nu_\mu$ channel. In Table 8, we give the opposite side mistag for signal and background events selected in the 33.9 M $\mathrm{b\overline{b}}$ sample. The opposite

[5]It is equal to the true mistag fraction measured using the Monte Carlo truth. Indeed, the muon or pion selected in the reconstruction of $\mathrm{B}^+ \to \overline{\mathrm{D}}^0\mu^+\nu_\mu$ or $\mathrm{B}^+ \to \overline{\mathrm{D}}^0\pi^+$ carry the right charge in 99% of the cases.

category	
Background (191 events)	$\omega^{\rm b}_{\rm OS}= 37.0 \pm 4.9\%$
Signal (255 event)	$\omega^{\rm s}_{\rm OS}= 30.5 \pm 3.8\%$
Total (446 event)	$\omega^{\rm tot}_{\rm OS}= 33.2 \pm 3.0\%$

Table 8: Opposite side mistag rate of the 446 $B^+ \Rightarrow \overline{D}^0\mu^+\nu_\mu$ candidates selected in the 33.9 M $b\overline{b}$ sample. It is estimated comparing the charge of the μ with the decision of the opposite side tagging algorithm.

side mistag fraction, $\omega^{\rm tot}_{\rm OS}$ depends on the opposite side mistag of signal and background, ($\omega^{\rm s}_{\rm OS}$, $\omega^{\rm b}_{\rm OS}$), as well as the B/S ratio:

$$\omega^{\rm tot}_{\rm OS} = \frac{\omega^{\rm s}_{\rm OS} + B/S \times \omega^{\rm b}_{\rm OS}}{1 + B/S}.$$

Therefore, measuring the mistag ignoring the background leads to a bias, which is, in the case of the $B^+ \Rightarrow \overline{D}^0\mu^+\nu_\mu$ channel: $\omega^{\rm tot}_{\rm OS} - \omega^{\rm s}_{\rm OS} = 2.7 \pm 3.8\%$.

We know that the $B^+ \Rightarrow \overline{D}^0\mu^+\nu_\mu$ background is $B^0 \rightarrow D^{*-}\mu^+\nu_\mu$ events, at 65%. A way to reduce the above bias is to perform a combined fit of the mistag rates of B^+ ($\omega^{\rm u}_{\rm OS}$) and B^0 ($\omega^{\rm d}_{\rm OS}$). For this, we build the following time-dependent asymmetry:

$$\mathcal{A}(t) = \frac{N_{\rm unmixed}(t) - N_{\rm mixed}(t)}{N_{\rm unmixed}(t) + N_{\rm mixed}(t)}$$

where $N_{\rm unmixed}(N_{\rm mixed})$ is the number of $B^+ \Rightarrow \overline{D}^0\mu^+\nu_\mu$ candidates where the *reconstructed* charge of the muon agrees (dis-agrees) with the result of the opposite side tagging algorithm; t is the proper time of the B candidates. Assuming $B^0 \rightarrow D^{*-}\mu^+\nu_\mu$ is the only background in $B^+ \Rightarrow \overline{D}^0\mu^+\nu_\mu$, ignoring proper time resolution and acceptance, we can write:

$$\mathcal{A}(t) = f_{\rm u}(1 - 2\omega^{\rm u}_{\rm OS}) + (1 - f_{\rm u})(1 - 2\omega^{\rm d}_{\rm OS})\cos(\Delta m_{\rm d} t),$$

where $f_{\rm u} = 1/(1 + \frac{B}{S})$ is the B^+ fraction in the sample. The time-dependent asymmetry for true $B^+ \rightarrow \overline{D}^0\mu^+\nu_\mu$ and $B^0 \rightarrow D^{*-}\mu^+\nu_\mu$ are shown on Fig. 26. The first one is fitted with $(1 - 2\omega^{\rm u}_{\rm OS})$ while the second one is fitted with $(1 - 2\omega^{\rm d}_{\rm OS})\cos(\Delta m_{\rm d} t)$. Clearly, we do not have enough statistics to conclude. Prospects to this study consist in showing that the B/S, together with the mistag fractions of B^+ and B^0 can be extracted from a fit to the combined asymmetry and to the invariant mass of the $\overline{D}^0\mu^+$ pair.

6 Conclusion

We have proposed two new charged B decay modes to measure the opposite mistag rate. With an integrated luminosity of $2\,{\rm fb}^{-1}$, the $B^+ \rightarrow \overline{D}^0\pi^+$ and $B^+ \Rightarrow \overline{D}^0\mu^+\nu_\mu$ channels

provide respectively 1 M and 2.4 M events triggered and offline selected. The B/S ratio are respectively 0.1 and 0.7. A luminosity of $0.1\,\mathrm{fb}^{-1}$ allows to measure the opposite side mistag ω_{OS} with a statistical uncertainty of 0.6%. Ignoring background leads to a systematics uncertainty of few percents. A combined fit of the mixing asymmetry of both B^+ and B^0 should allow to extract the two mistag rates, provided the B/S can be extracted from side-bands of the mass distributions.

Acknowledgments

We would like to thank Marta Calvi for fruitful discussions, especially about the $\mathrm{B}^0 \to \mathrm{D}^{*-}\mu^+\nu_\mu$ channel. We would also like to thank Patrick Robbe for his help in the Monte Carlo generators.

References

[1] M. Calvi *et al.*, "LHCb flavour tagging performance", LHCb/2003–115.

[2] A. Golutvin, R. Hierck, J. van Hunen, M. Prokudin and R. White, "$\mathrm{B}_\mathrm{s}^0 \to \mathrm{D}_\mathrm{s}^\mp \mathrm{K}^\pm$ and $\mathrm{B}_\mathrm{s}^0 \to \mathrm{D}_\mathrm{s}^- \pi^+$ event selection", LHCb/2003–127.

[3] G. Raven, "Selection of $\mathrm{B}_\mathrm{s}^0 \to \mathrm{J}/\psi\phi$ and $\mathrm{B}^+ \to \mathrm{J}/\psi\mathrm{K}^+$", LHCb/2003–118.

[4] J. Babel, "Analysis of a non standard sZb coupling scenario – Flavour tagging in LHCb", PhD thesis, 2006.

[5] Particle Data Group, Phys. Letters **B592** (2004) 1.

[6] T. Sjöstrand *et al.*, Computer Physics Commun. **135** (2001) 238.

[7] D. Lange, "The EvtGen particle decay simulation package", Nucl. Inst. and Methods **A462** (2001) 152.

[8] GEANT 4 collaboration, Nucl. Inst. and Methods **A 506** (2003), 250. http://geant4.cern.ch/geant4

[9] http://lhcb-comp.web.cern.ch/lhcb-comp/Simulation/default.htm

[10] http://lhcb-comp.web.cern.ch/lhcb-comp/Digitization/default.htm

[11] http://lhcb-comp.web.cern.ch/lhcb-comp/Reconstruction/default.htm

[12] http://lhcb-comp.web.cern.ch/lhcb-comp/Analysis/default.htm

[13] http://lhcb-comp.web.cern.ch/lhcb-comp/Analysis/Bender/index.html

[14] LHCb Collaboration "LHCb Reoptimized Detector Technical Design and Performance", CERN/LHCC 2003-030, 9 September 2003.

[15] H. Dijkstra *et al* "Some Remarks on Systematic Effects of the Trigger and Event Generator Studies", LHCb/2003–157.

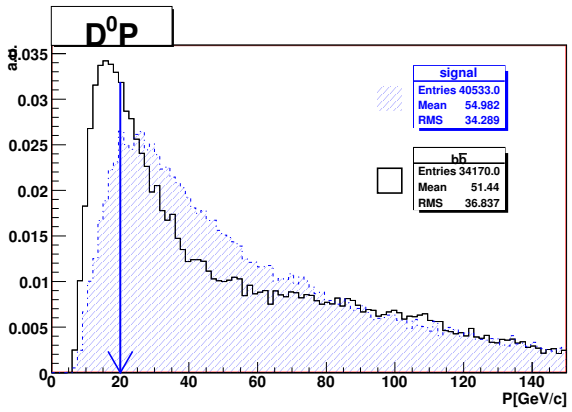

Figure 3: Momentum distribution of the $\overline{D}^0$ candidate in $B^+ \to \overline{D}^0\pi^+$ and $b\overline{b}$ events. In all the following plots, the distribution of signal and background is normalized to unity, for comparison. That is why the vertical axis is label with arbitrary units (a.u.).

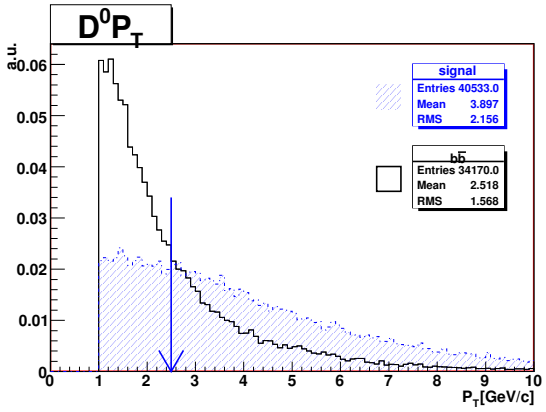

Figure 4: Transverse momentum distribution of the $\overline{D}^0$ candidate in $B^+ \to \overline{D}^0\pi^+$ and $b\overline{b}$ events.

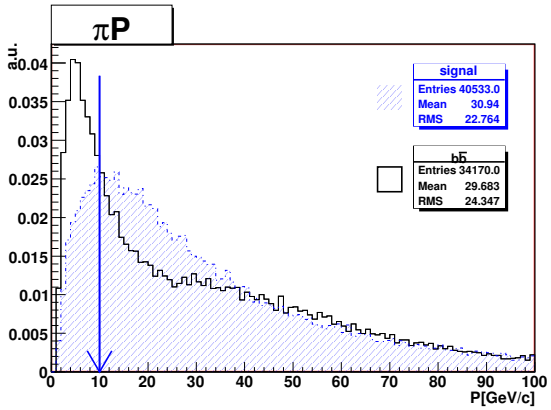

Figure 5: Momentum distribution of the π_1 candidate in $B^+ \to \overline{D}^0\pi^+$ and $b\overline{b}$ events.

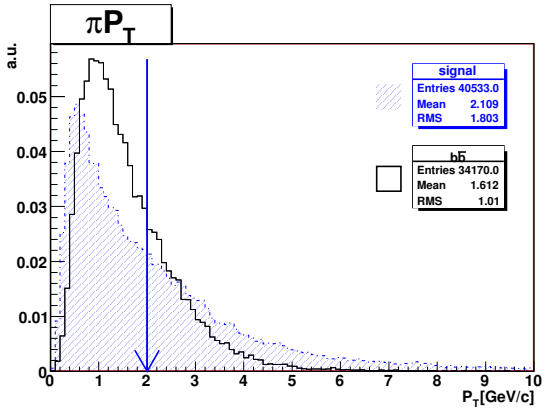

Figure 6: Transverse momentum distribution of the π_1 candidate in $B^+ \to \overline{D}^0\pi^+$ and $b\overline{b}$ events.

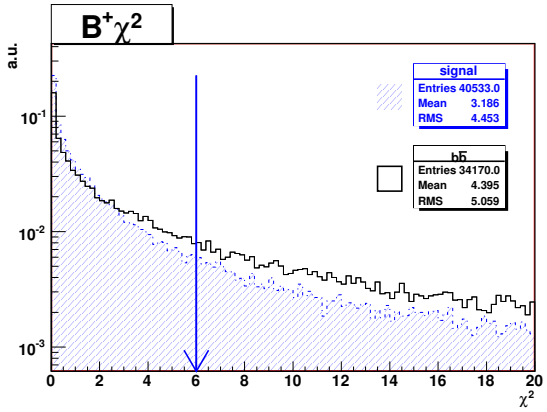

Figure 7: χ^2 of an unconstrained vertex fit to the $\overline{\mathrm{D}}^0\pi^+$ pair, in $\mathrm{B}^+ \to \overline{\mathrm{D}}^0\pi^+$ and $\mathrm{b\overline{b}}$ events.

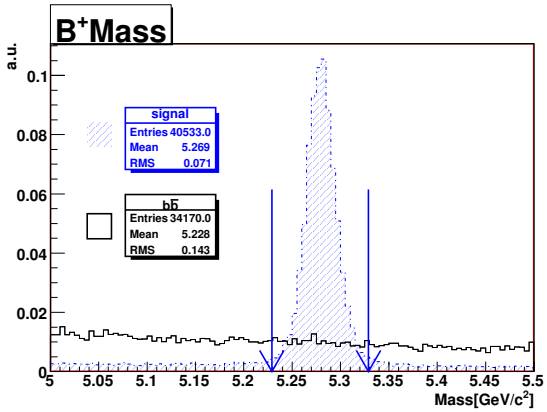

Figure 8: Invariant mass of the $\overline{\mathrm{D}}^0\pi^+$ pair, in $\mathrm{B}^+ \to \overline{\mathrm{D}}^0\pi^+$ and $\mathrm{b\overline{b}}$ events.

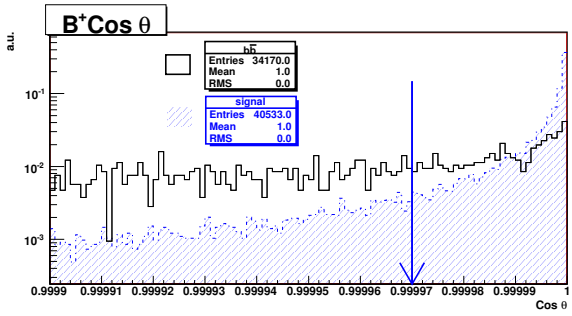

Figure 9: $\cos\theta$ distribution in $\mathrm{B}^+ \to \overline{\mathrm{D}}^0\pi^+$ and $\mathrm{b\overline{b}}$ events.

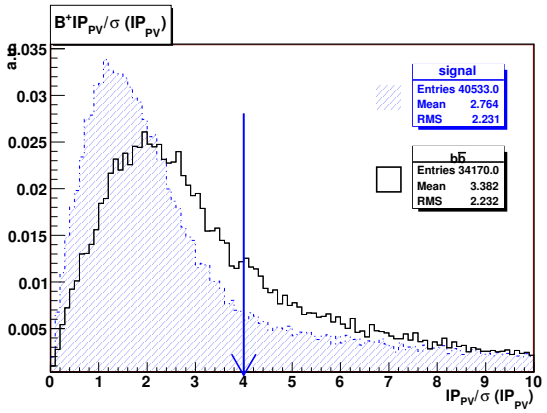

Figure 10: Impact parameter significance of the $\mathrm{B}^+ \to \overline{\mathrm{D}}^0\pi^+$ candidates with respect to the primary vertex, $\mathrm{ip_{PV}}/\sigma(\mathrm{ip_{PV}})(\overline{\mathrm{D}}^0\pi)$ in $\mathrm{B}^+ \to \overline{\mathrm{D}}^0\pi^+$ and $\mathrm{b\overline{b}}$ events.

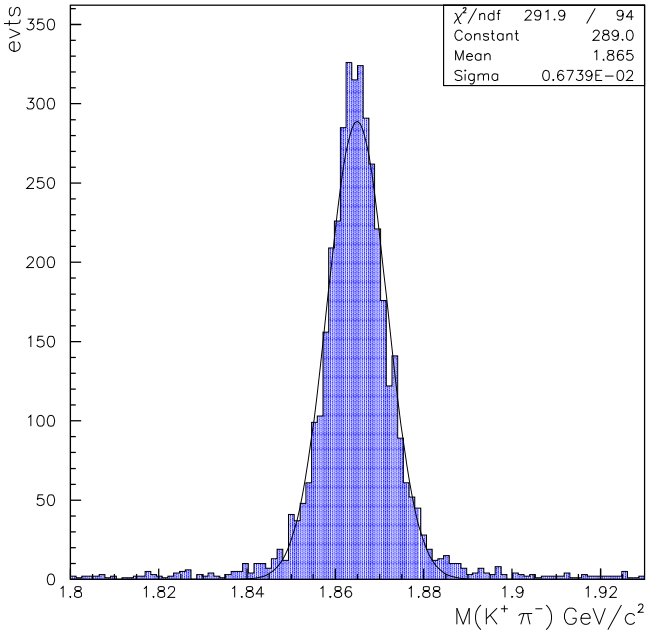

Figure 11: Invariant mass of the Kπ pairs. It is centered on the $\overline{\mathrm{D}}^0$ mass and the resolution is 6.8 MeV/c^2.

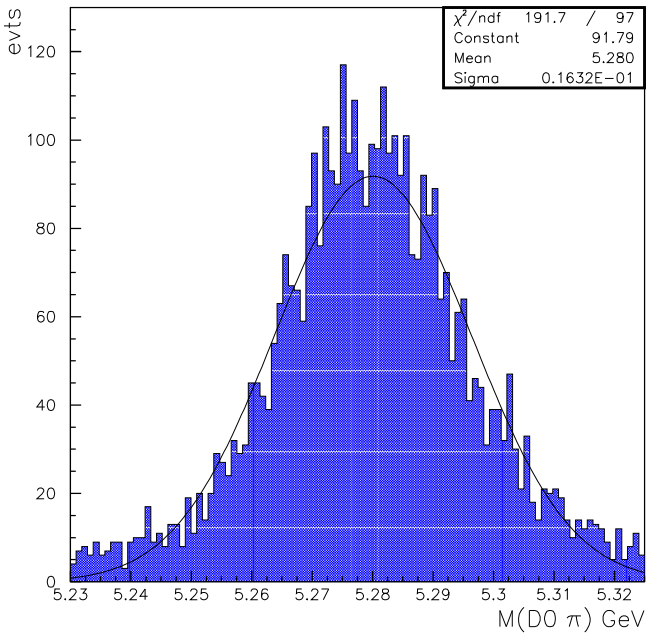

Figure 12: Invariant mass distribution of $\overline{\mathrm{D}}^0\pi^+$ pair, on the $\mathrm{B}^+ \to \overline{\mathrm{D}}^0\pi^+$ sample. It is centered on the B^+ mass (=5.279 GeV/c^2) and the resolution is 16.3 MeV/c^2.

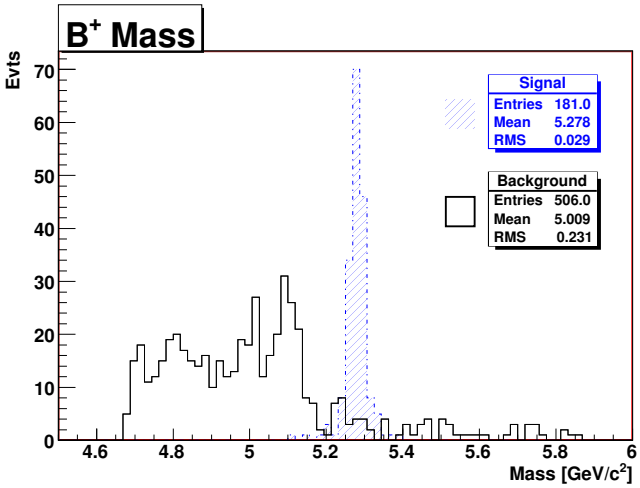

Figure 13: Invariant mass distribution of $\overline{\mathrm{D}}^0\pi^+$ pair, in the $\mathrm{b\overline{b}}$ sample. The signal peack is clearly visible, centered on the B^+ mass (=5.279 GeV/c^2). The contribution from partially reconstructed decays appears in the lower mass region.

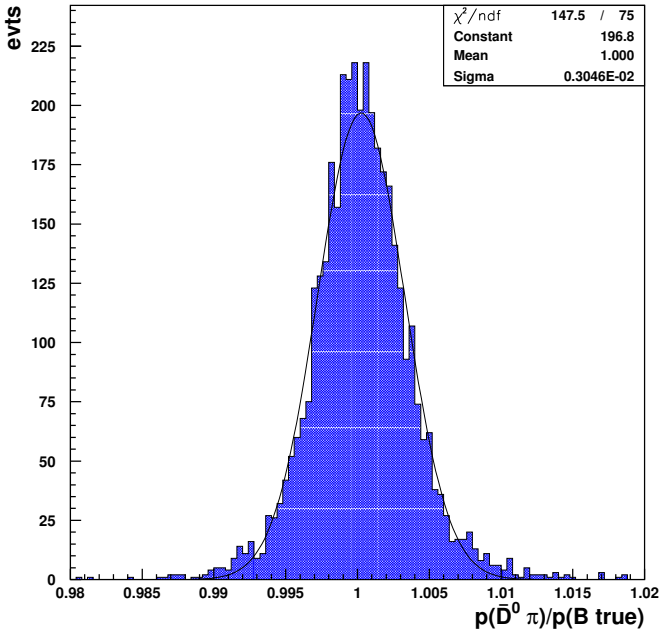

Figure 14: Momentum resolution of $B^+ \to \overline{D}^0 \pi^+$ candidates. $\sigma(p)/p = 0.3\%$

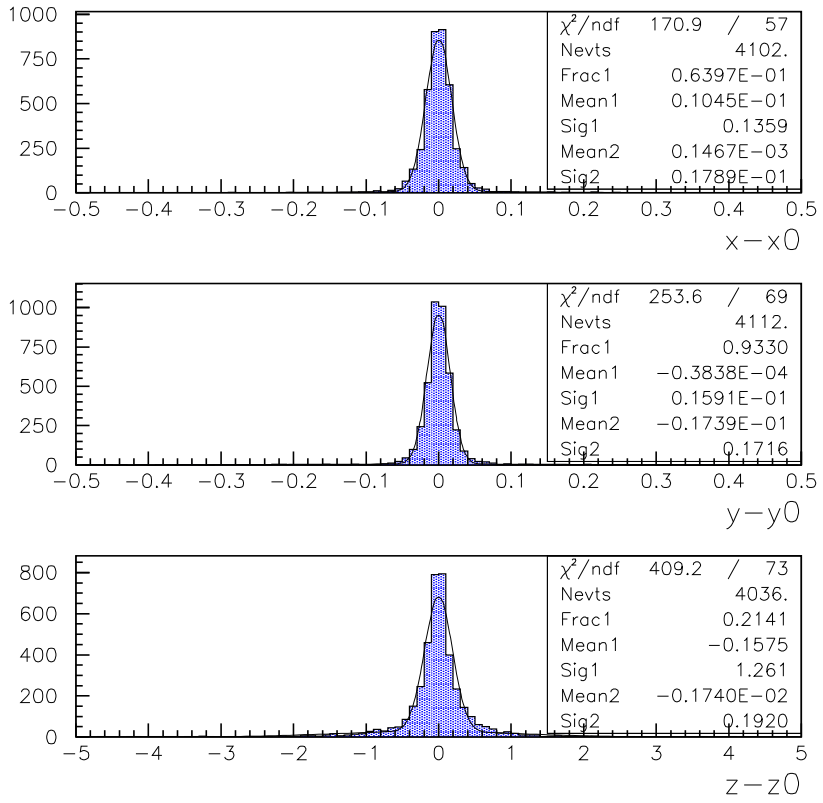

Figure 15: Resolution of the reconstructed B^+ vertex along the x, y, z axis, in $B^+ \to \overline{D}^0\pi^+$ events.

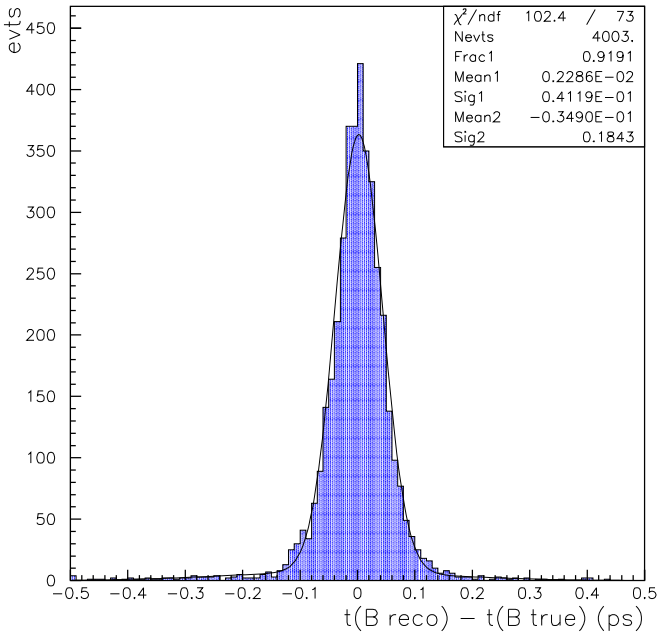

Figure 16: $B^+ \to \overline{D}^0\pi^+$ proper time resolution, fitted by the sum of two Gaussians. The standard deviation of the core is 41 fs.

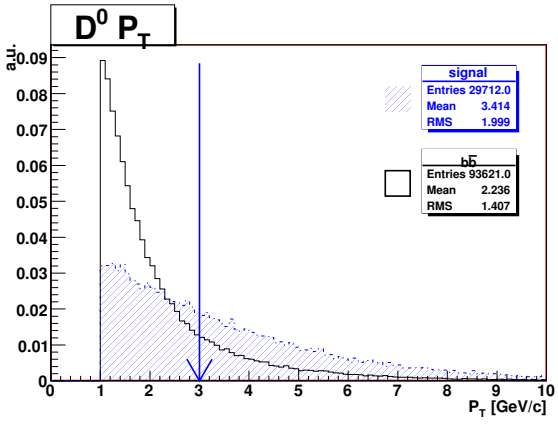

Figure 17: Transverse momentum distribution of the $\overline{D}^0$ candidate in $B^+ \to \overline{D}^0\mu^+\nu_\mu$ and $b\overline{b}$ events.

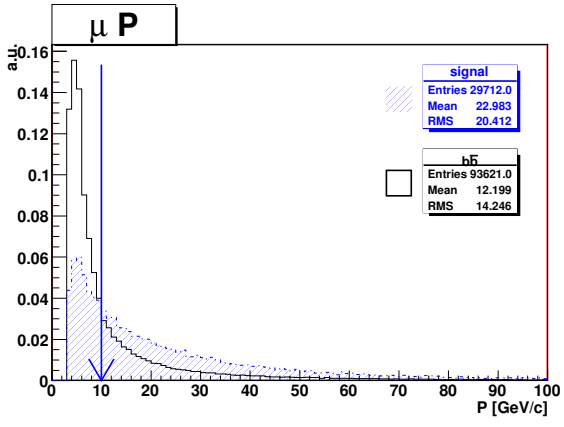

Figure 18: Momentum distribution of the μ candidate in $B^+ \to \overline{D}^0\mu^+\nu_\mu$ and $b\overline{b}$ events.

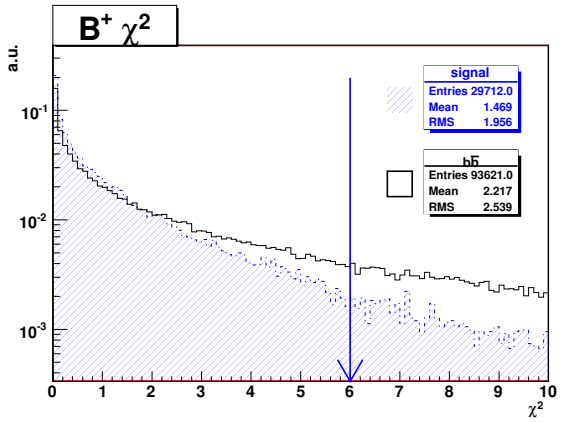

Figure 19: χ^2 of an unconstrained vertex fit to the $\overline{\mathrm{D}}^0\mu^+$ pair, in $\mathrm{B}^+ \to \overline{\mathrm{D}}^0\mu^+\nu_\mu$ and $\mathrm{b\bar{b}}$ events.

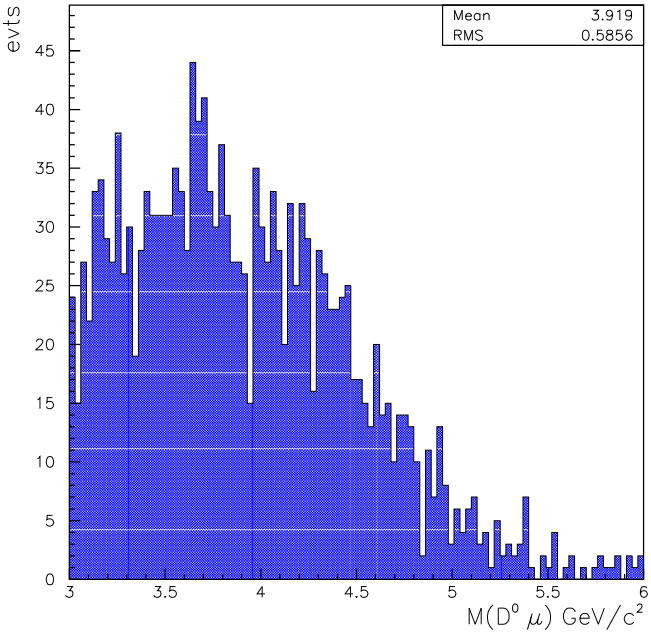

Figure 20: Invariant mass of the $\overline{\mathrm{D}}^0\mu^+$ pair, in the $\mathrm{B}^+ \to \overline{\mathrm{D}}^0\mu^+\nu_\mu$ sample.

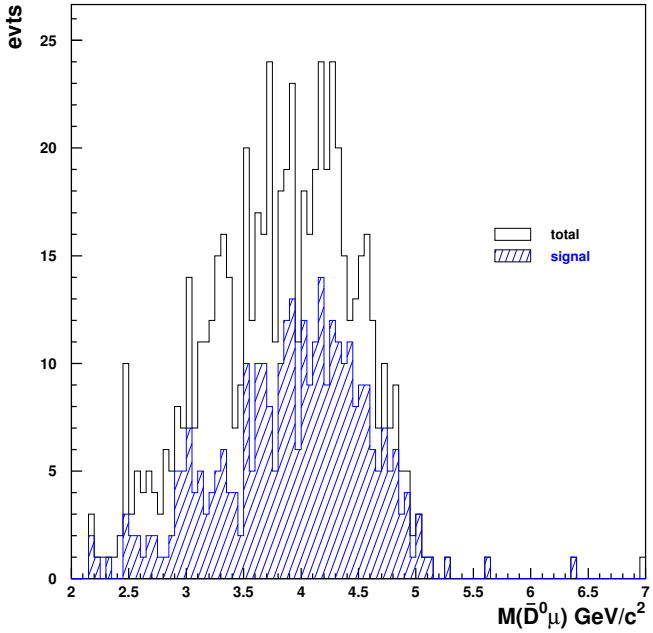

Figure 21: Invariant mass distribution of $\overline{\mathrm{D}}^0\mu^+$ pair, in the $\mathrm{b\overline{b}}$ sample. The true $\mathrm{B}^+ \Rightarrow \overline{\mathrm{D}}^0\mu^+\nu_\mu$ signal events are also indicated.

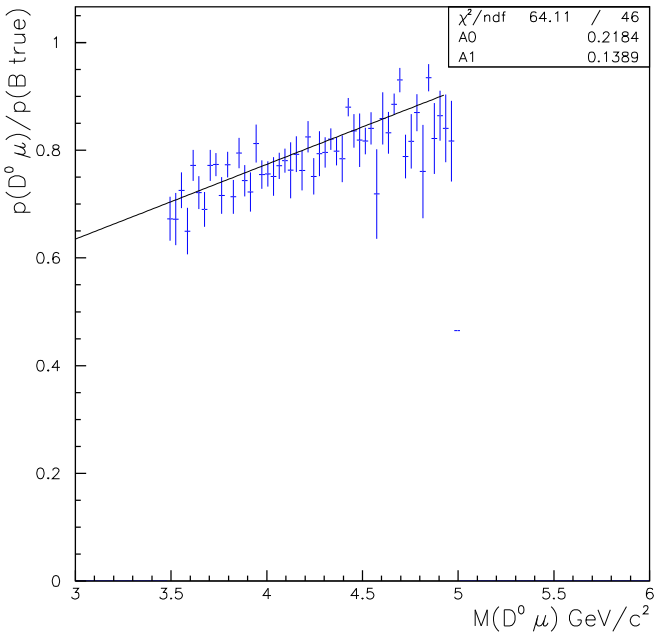

Figure 22: $p(\overline{D}^0\mu^+)/p(B\,\text{true})$ as a function of the $\overline{D}^0\mu^+$ invariant mass, fitted with a first-order polynomial function

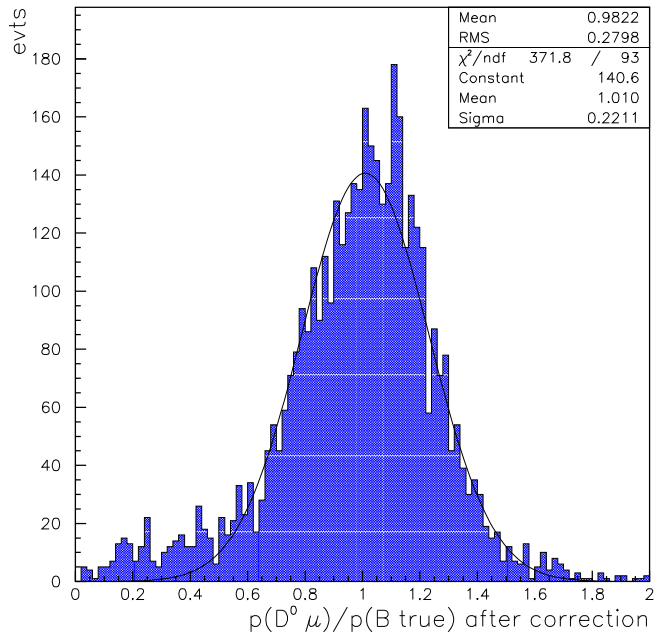

Figure 23: $B^+ \to \overline{D}^0\mu^+\nu_\mu$ momentum resolution after correcting for the missing neutrino.

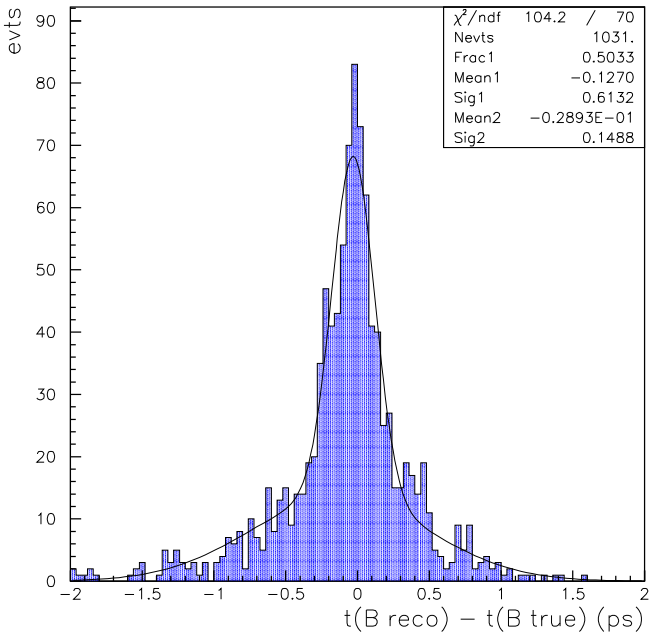

Figure 24: $B^+ \to \overline{D}^0 \mu^+ \nu_\mu$ proper time resolution, fitted with a sum of two Gaussians. The standard deviation of the core is 149 fs

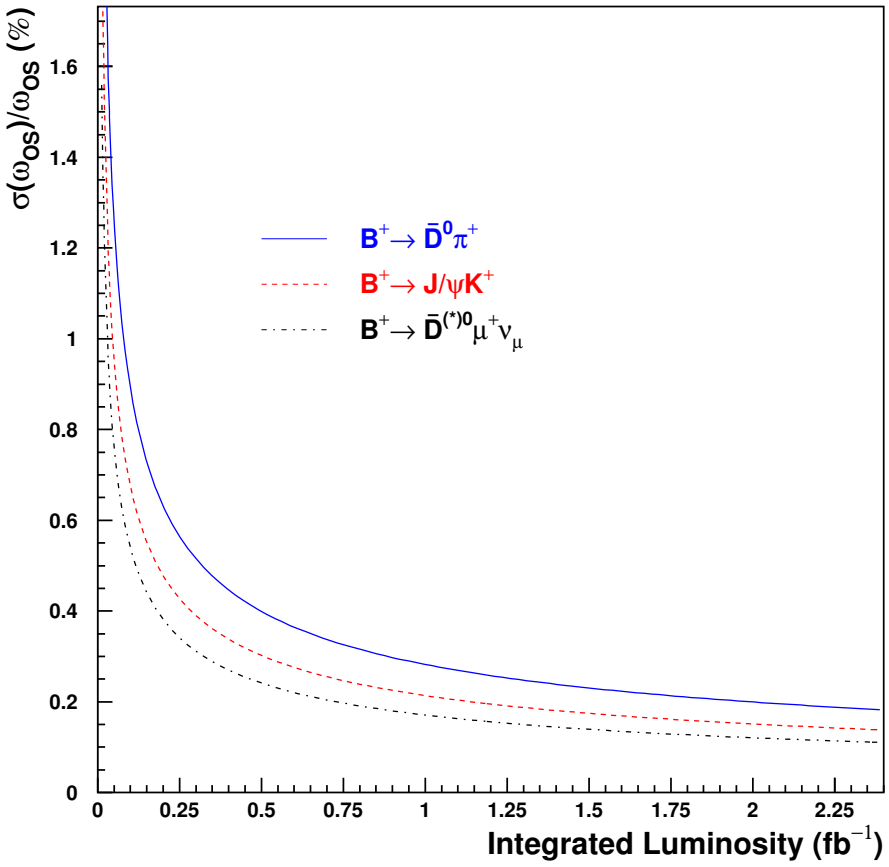

Figure 25: Relative uncertainty on the opposite side mistag rate as a function of the integrated luminosity, for the three charged modes: $B^+ \to \overline{D}^0\pi^+$, $B^+ \to J/\psi K^+$ and $B^+ \Rightarrow \overline{D}^0\mu^+\nu_\mu$. The background is not taken into account.

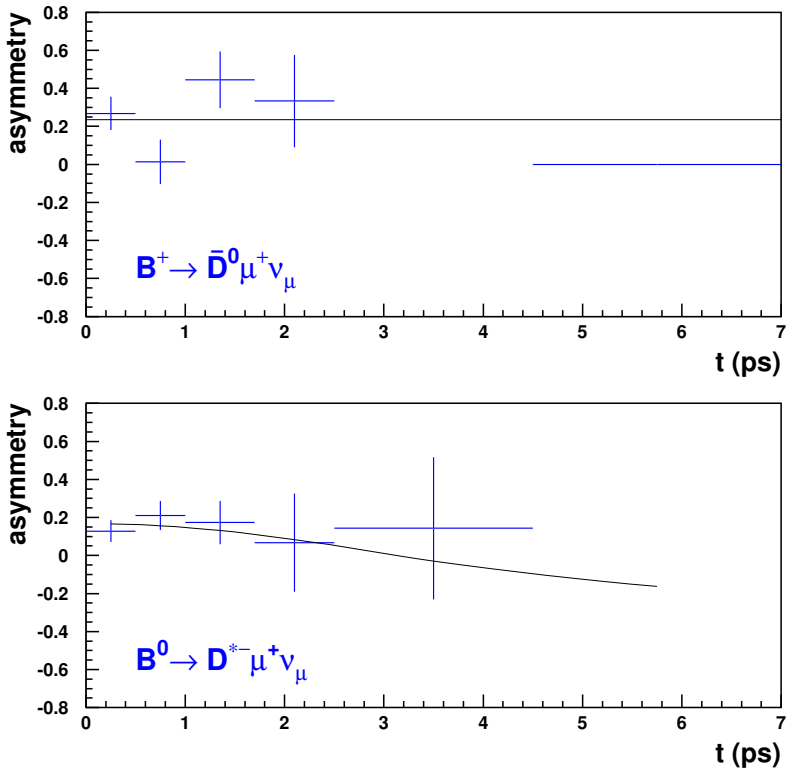

Figure 26: Mixing asymmetry of $B^+ \to \overline{D}^0 \mu^+ \nu_\mu$ and $B^0 \to D^{*-} \mu^+ \nu_\mu$ as a function of proper time; fitted with a 0-degree polynom for the first one $(1-2\omega^{u}_{OS})$ and $(1-2\omega^{d}_{OS})\cos(\Delta m_d t)$ for the second, with Δm_d=0.502 ps^{-1}.